



Effects of Relief Hole on the Static Characteristics of Externally Pressurized Steam-Lubricated Hybrid Journal-Thrust Bearing

Zhansheng Liu, Jinlei Qi^(✉), Xiangyu Yu, Peng He, Bing Han, Yishun Yang, and Jiaqi Wang

Harbin Institute of Technology, Harbin 08544, NJ, China
qijinlei@stu.hit.edu.cn

Abstract. In order to improve the static performance of externally pressurized steam hybrid journal-thrust bearing (EPSHJTB), this study proposes a novel relief hole structure. First, based on the classical bearing experimental data, the correctness of simulation method is verified. The detailed flow analysis of hybrid bearing is conducted using the computational fluid tool. Flow field variables are presented which include pressure, temperature and etc. Second, the relief hole structure is designed to reduce the radial and axial film outlet pressure. This study compares the static load capacity of EPSHJTB with and without relief holes. It's found that the relief holes actually improve the load capacity of bearing. The numerical results also show that the position of relief holes influence the pressure distribution.

Keywords: Externally-Pressurized Steam Lubrication · Hybrid Journal-Thrust Bearing · Static performance · Load capacity

1 Introduction

With the development of high power density and closed-cycle steam turbines in deep-sea exploration missions, studies on process fluid lubrication represent a growing field due to its numerous advantages [1, 2]. Externally pressurized steam-lubricated bearing is one of the key components of process fluid lubrication, which plays a crucial role in oil-free and closed-cycle steam turbines. Understanding how bearing geometrical structure and parameters affect the bearing overall performance is in importance in light of practical application.

A considerable amount of literature has been published on improving the load capacity of externally pressurized gas bearing. Structure design is the fundamental direction for bearing optimization. Mori [17] conducted a detailed theoretical analysis of aerostatic thrust bearing and pointed out that the conical cavity structure could improve the load capacity of aerostatic thrust bearing. Du et al. [14] considered the effect of pressure equalizing grooves on aerostatic journal bearing. Li et al. [15, 16] proposed a backflow

channel aerostatic thrust bearing with shunt injection to increase the load capacity and stiffness.

In order to further reduce the structure size and improve machine power density, numerous researchers have tried to combine thrust bearings and journal bearings. The previous patent by Yates [4] demonstrated a journal-thrust hybrid bearing which made use of leakage flow from journal bearing to supply thrust bearing. This novel design has obvious advantages such as decreasing the total mass flow and simplifying the whole system [3]. Zhang [11] designed a new gas flow path for aerostatic hybrid bearing in ultra-precision spindle and concluded that hybrid bearing could achieve effective lubrication. Lu et al. [9, 10] researched the fluid-structure interaction effect on the hybrid bearing characteristics and also found that aerostatic spindle could be supported readily.

Taken together, these studies support the notion that improving the load capacities of hybrid journal-thrust bearing is fundamental for machine reliability. However, there is a relatively few studies on the relief hole. Work is needed to fully understand the implications and effects of relief hole. This paper researches the EPSHJTBB based on CFD-numerical method. On the basis of flow and heat transfer of the EPSHJTBB, a novel relief hole structure and hollow shaft concept are proposed to improve the load capacity. A further study on relief hole geometrical parameters is also conducted.

2 Numerical Method

2.1 Geometry Model and Mesh

Externally pressurized steam hybrid journal-thrust bearing (EPSHJTBB) makes use of high temperature and high pressure superheated steam as the lubricating medium. Superheated steam flows through 3 rows of radial throttle orifices and 1 row of axial throttle orifices and finally forms continuous lubricating film, as shown in Fig. 1. The axial relief holes are distributed uniformly on the shaft circular plate. And the radial relief holes are distributed uniformly on the shaft surface. The thickness and pressure distribution of the lubricating film will be nonuniform due to shaft eccentricity. Geometric parameters of the EPSHJTBB are presented in Table 1.

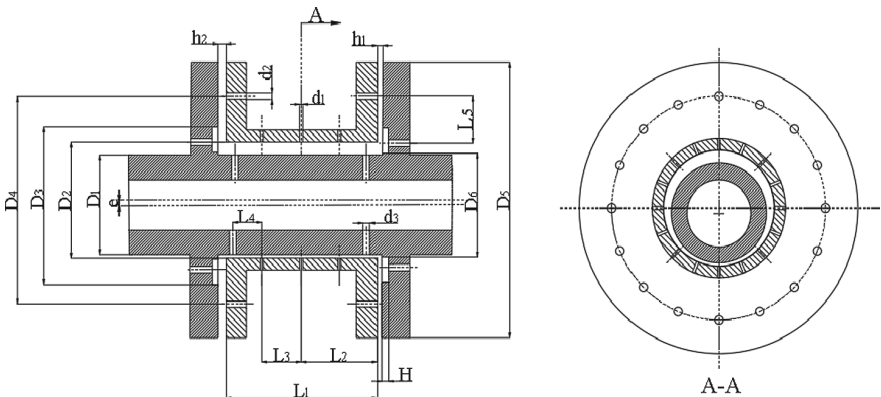


Fig. 1. Externally pressurized steam journal-thrust bearing sketch

Table 1. Geometric parameters of EPSHJT

Parameter	Value
Diameter of the journal D_1	109.924 mm
Diameter of the bearing D_2	110 mm
Average radial film thickness c	0.038 mm
Axial film thickness h_1/h_2	0.0075 mm/0.0225 mm
Outer diameter D_5	220 mm
Distribution Circle Diameter D_4	165 mm
Length of the bearing L_1	110 mm
Diameter of the orifice d_1	2 mm
Diameter of the orifice d_2	2 mm
Radial Position L_5	25 mm
Axial Position L_4	10 mm
Axial Position L_3	40 mm
Axial Position L_2	55 mm
Diameter of the relief hole d_3	3 mm
Eccentricity ratio /Eccentricity distance e	0.5/0.019 mm
Number of radial orifices	3x16
Number of axial orifices	1x16 each thrust face
Number of axial relief holes	1x16 each thrust face
Number of radial relief holes	2x16
Groove depth H	1 mm
Groove outer diameter D_3	120 mm
Groove inner diameter D_6	111 mm

The relief hole structure is demonstrated in Fig. 2. Radial relief holes and thrust relief holes are marked. Model A is one sixteenth of the whole fluid domain and model B is one half of the radial bearing part. There are 2 radial relief holes and 2 thrust relief holes in model A. Besides, there exist 2 relief grooves in model A. And there are 18 radial relief holes in model B.

The fluid domain and mesh details are displayed in Fig. 3. Based on the ICEM CFD 19.0, structured multiblock grids are adopted to decrease the total mesh number of the computational fluid domain, considering the large dimensional difference between film thickness direction and circumferential/axial direction. O-blocks are created in order to improve the mesh quality. Meshes are locally refined around throttle orifices. The mesh convergence test result is shown in Table 2. The node number in the film height direction is more important than the axial node number and circumferential node number, which affects significantly the load capacity result. When the node number in the film

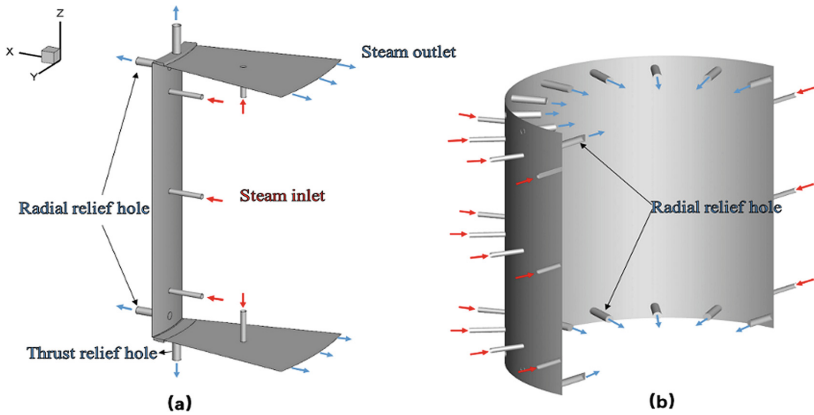


Fig. 2. EPSHJT fluid domain with relief hole structure: **a** Model A; and **b** Model B

height direction reaches 14, the load capacity changes slowly and tends towards stable. Therefore, an appropriate node distribution is adopted and there are 13 layers in film thickness direction. With regard to model A, the total nodes number is 1589772 and the total elements number is 1670526. The axial node number is 360 and the circumferential node number is 60. The minimum determinant $3 \times 3 \times 3$ value is above 0.77 and mesh quality is above 0.60 for model A. With regard to model B, the total nodes number is 6958980 and the total elements number is 7304888. The axial node number is 320 and the circumferential node number is 640. The minimum determinant $3 \times 3 \times 3$ value is above 0.60 and mesh quality is above 0.55 for model B.

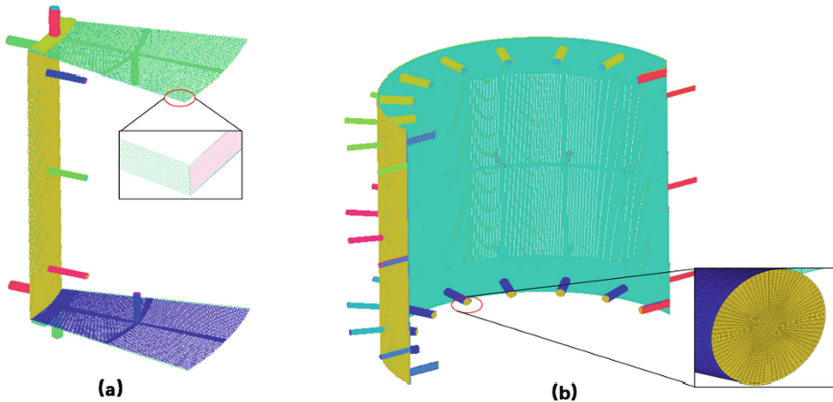


Fig. 3. EPSHJT fluid domain mesh details: **a** Model A; and **b** Model B

2.2 Properties of Steam

Figure 4 presents the pressure-temperature diagram of steam with various pressures and temperatures. This graph shows that the real properties of steam according to Coolprop

Table 2. Mesh Convergence

Mesh Model	Mesh Number	Aixal Node Number	Circumferential Node Number	Film Hegiht Node Number	Load Capacity
Model A	1431438	360	60	4	1060.333 N
	1527198	360	60	8	728.995 N
	1670526	360	60	14	516.187 N
	1790538	360	60	19	474.169 N
	1862358	360	60	22	472.291N
Model B	4830258	320	640	4	842.325 N
	1432460	160	320	8	981.865 N
	4775560	210	400	8	1043.873 N
	5820110	320	640	8	1009.769 N
	6562499	320	640	11	1250.012N
	7304888	320	640	14	1396.605 N
	8542203	320	640	19	1476.220 N
	9284592	320	640	22	1384.252 N

database [20]. It is apparent that the inlet steam is superheated and the degree of superheat is 66.15 K.

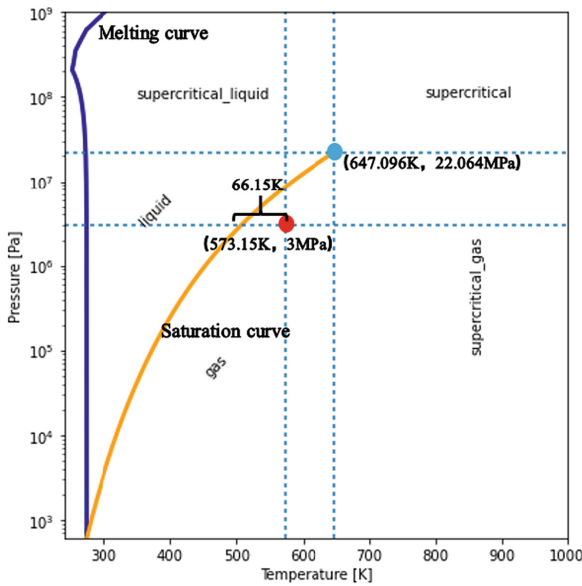


Fig. 4. Pressure-temperature diagram of steam

Table 3 lists the thermodynamic properties of steam. The dynamic viscosity and thermal conductivity are assumed to be constant which don't vary with temperature and pressure changing. Redlich-Kwong Equation is adopted as the steam equation of state.

Table 3. Properties of steam

Lubricant-Steam	Value
Temperature	573.15K
Pressure	3 MPa
Dynamic viscosity	1.34x10 ⁻⁵ Pa·s
Thermal conductivity	26.1 W/(m·K)

Standard Redlich-Kwong Equation:

$$P = \frac{RT}{V-b} - \frac{\alpha_0}{V(V+b)T^{0.5}} \quad (1)$$

$$\alpha_0 = 0.42748 \frac{R^2 T_c^{2.5}}{P_c} \quad (2)$$

$$b = 0.08664 \frac{RT_c}{P_c} \quad (3)$$

where R is gas constant, T_c is critical temperature and P_c is the critical pressure.

2.3 Numerical Model and Verification

The numerical simulations in this article are conducted on ANSYS FLUENT 19.0. Based on previous numerical studies, we use realizable k-epsilon turbulence model and standard wall function. The convergence residual criteria for continuity, momentum and energy are all set to 10⁻⁶. The solution algorithm for pressure-velocity coupling is SIMPLE. Steady absolute pressure-based solver is adopted. The governing equations are discretized with the second-order upwind scheme in density/momentum/energy, with the second-order scheme in pressure, while with the first upwind scheme in turbulent kinetic energy and turbulent dissipation. The gradient is discretized by least squares cell-based method.

Continuity equation:

$$\frac{D\rho}{Dt} + \rho \nabla \cdot \vec{u} = \frac{\partial \rho}{\partial t} + \nabla \cdot (\rho \vec{u}) = 0 \quad (4)$$

Momentum equation:

$$\frac{\partial(\rho \vec{u})}{\partial t} + \nabla \cdot (\rho \vec{u} \vec{u}) = -\nabla p + \nabla \cdot \tau \quad (5)$$

Energy equation:

$$\frac{\partial(\rho h^*)}{\partial t} - \frac{\partial p}{\partial t} + \nabla \cdot (\rho U h^*) = \nabla \cdot (\lambda \nabla T) + \nabla \cdot (U \cdot \tau) \tag{6}$$

As shown in Table 4, no-slip velocity condition and adiabatic condition are imposed on all walls. The inlet total pressure is equal to 3 MPa and inlet total temperature is equal to 573.15 K. The inlet turbulent intensity is set to 5% and the inlet turbulent viscosity ratio is set to 10. The outlet pressure is assumed to be 0 and outlet temperature is assumed to 300 K.

Table 4. Boundary conditions

Position	Boundary Conditions
Inlet	Gauge total pressure is 3 MPa, Total temperature is 573.15 K, Supersonic and initial pressure is 0;
Outlet	Pressure is 0, Temperature is 300 K
Wall	No slip and static wall without heat flux

The externally pressurized steam-lubricated journal bearing static performance is characterized by load capacity and mass flow rate. In this study, such an approximate method is adopted to calculate the load capacity of EPSHJT B: calculate the axial load capacity by using the thrust gas film pressure distribution of model A and calculate the radial load capacity by using the radial gas film pressure distribution of model B. Besides, we calculate the mass flow rate by using the inlet flow of model A.

Axial Load Capacity:

$$F_{axial} = 16 \int_{\text{mod } el-A} P \cdot dS \tag{7}$$

Radial Load Capacity:

$$F_{radial} = 2 \int_{\text{mod } el-B} P \cdot dS \tag{8}$$

Mass Flow Rate:

$$\dot{m} = 16 \int_{\text{mod } el-A} \rho \vec{u} \cdot dS \tag{9}$$

In this study, we compare the distribution of gas film pressure [7]. Based on the Fig. 5, we find that Realizable k-epsilon turbulence can capture the pressure depression phenomenon and the pressure distributions are similar. The reason for the deviations is the influence of throttle orifice inlet length and structure difference. The orifice inlet geometry will change the gas flow field such as pressure and velocity distribution, so the final gas film distribution will be influenced.

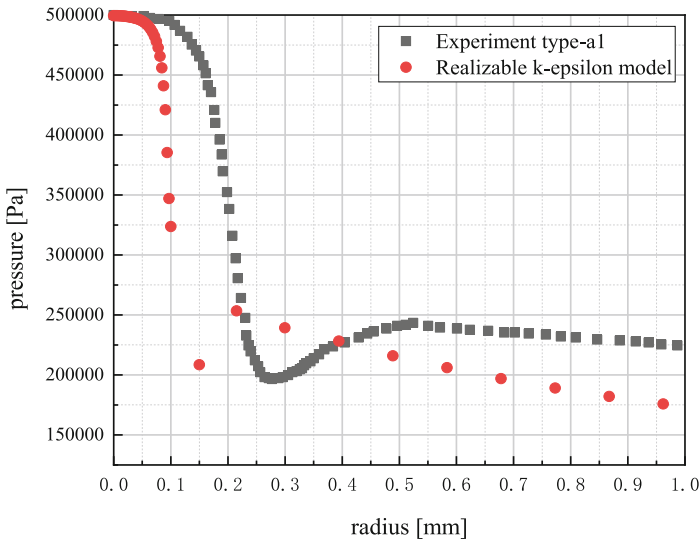


Fig. 5. Curve of radial pressure distribution: **a** Whole radius; and **b** Enlarged view

3 Results and Discussion

3.1 Traditional Externally Pressurized Steam Hybrid Journal-Thrust Bearing

This section focuses on investigating the flow and heat transfer characteristics of traditional hybrid journal-thrust steam bearing (EPSHJT_B), which includes pressure distribution and temperature distribution. The purpose of this section is to show load capacity generation mechanism.

Figure 6 depicts the pressure distribution of whole fluid domain. It can be seen that the radial gas film pressure is uniform due to high outlet back pressure. Therefore, the radial load capacity is nearly zero.

Figure 7 indicates the pressure distribution of main thrust face and auxiliary thrust face along the radial direction. The pressure of thrust gas film fluid domain near the radial gas film domain has the higher pressure than near the outlet. The pressure of main thrust face gas film is 2.9961 MPa. And the pressure of auxiliary thrust face gas film is 2.8803 MPa. It can be seen that the pressure suddenly drops near the throttle orifice of the auxiliary thrust face from 3 MPa to 2.2917 MPa and 2.5562 MPa. This pressure depression phenomenon is related to the clearance value [17, 18]. When the clearance is 7.5 μm , the pressure depression phenomenon is disappeared such as the main thrust face. The axial load capacity is generated due to the pressure distribution difference between main thrust face and auxiliary thrust face.

Figure 8 shows the temperature distribution of main thrust face and auxiliary thrust face. It can be seen that the temperature distribution is similar to pressure distribution. The temperature of main thrust face gas film near the radial part is 572.95 K. And the temperature of auxiliary thrust face gas film near the radial part is 571.85 K. The similar temperature depression phenomenon is also observed near the throttle orifice of the

auxiliary thrust face. The temperature drops from 573.15 K to 557.74 K near the outlet and drops from 573.15 K to 564.49 K near the radial gas film.

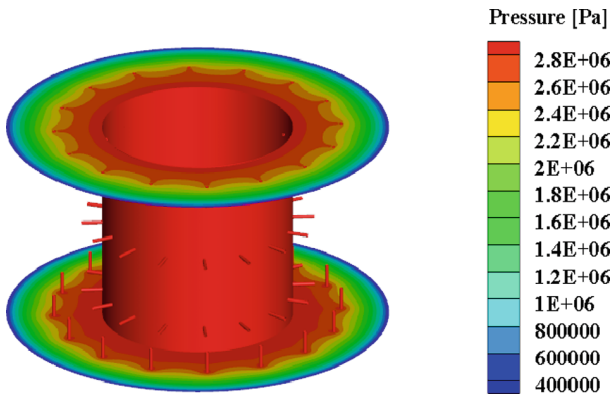


Fig. 6. Pressure distribution contour of traditional EPSHJT B

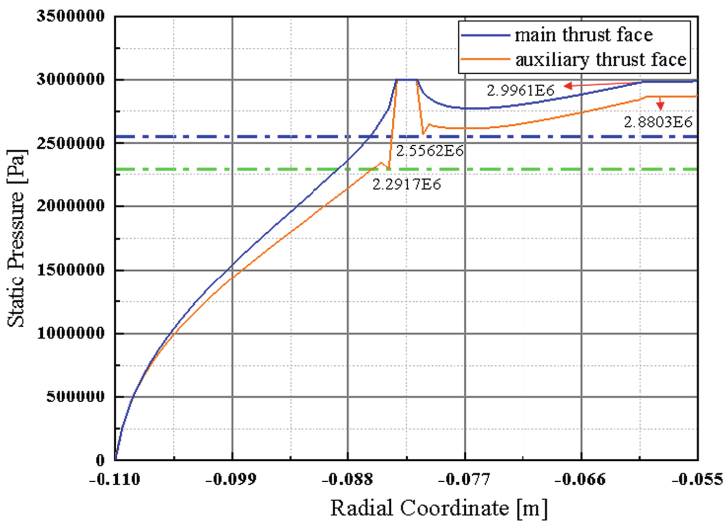


Fig. 7. Curve of thrust film pressure distribution

3.2 Externally Pressurized Steam Hybrid Journal-Thrust Steam Bearing with Relief Holes

This section focuses on investigating the flow characteristics of EPSHJT B with relief holes, which includes pressure distribution. The purpose of this section is to show the difference between traditional EPSHJT B and EPSHJT B with relief holes. Radial relief holes and thrust relief holes are all opened in EPSHJT B with relief holes.

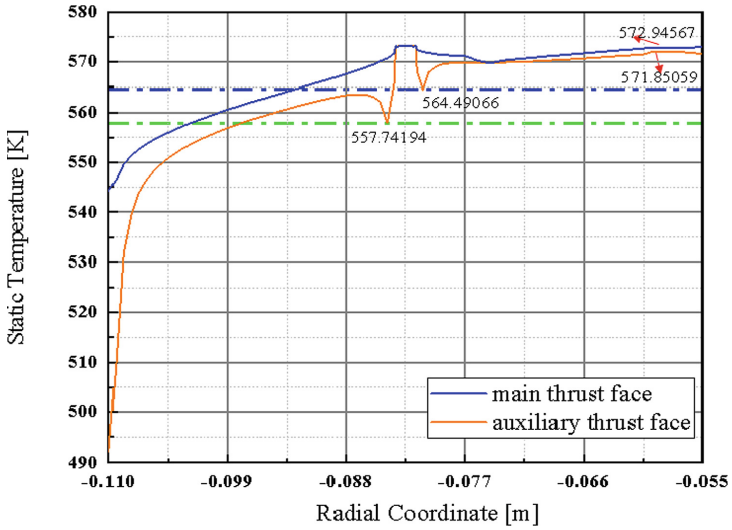


Fig. 8. Curve of thrust film temperature distribution

Figure 9 presents the pressure distribution contour of model A. It is apparent from this figure that thrust relief hole and groove structure can effectively reduce the outlet back pressure. Figure 10 presents the pressure distribution contour of model B. This figure illustrates how radial relief holes lower the radial gas film outlet pressure.

Figure 11 compares the pressure distribution between traditional EPSHJTБ and EPSHJTБ with relief holes. It can be seen that the new EPSHJTБ’s pressure difference between thrust faces is larger than traditional EPSHJTБ’s. The pressure of thrust relief hole and groove structure domain is nearly zero. As shown in Table 5, the load capacity and mass flow rate of EPSHJTБ with relief holes is higher than traditional

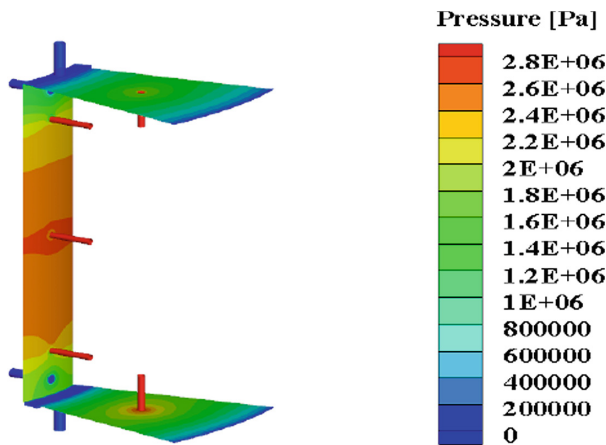


Fig. 9. Pressure distribution contour of EPSHJTБ with relief holes-model A

EPSHJTB. Besides, the radial load capacity of EPSHJTB with relief holes is produced by eccentricity.

Figure 12 displays the circumferential pressure distribution of the model B, which is in the axial middle position of the radial gas film. When the angle equals 0 and 180 degrees separately, the clearance film thickness value is the biggest and the smallest accordingly. Therefore, the gas film pressure reaches the lowest and highest respectively.

In order to improve the load capacity of thrust bearing part and radial bearing part, the thrust bearing and radial bearing outlet back pressure should be lowered.

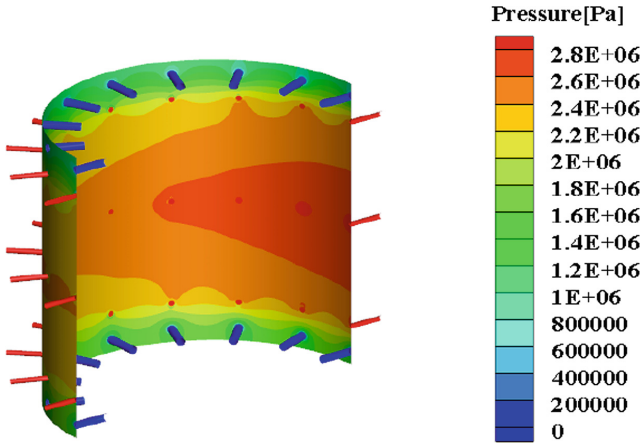


Fig. 10. Pressure distribution contour of EPSHJTB with relief holes-model B

3.3 Effects of Relief Holes Distribution

This section focuses on investigating the effects of relief hole distribution. The purpose of this section is to show the static characteristic variations between EPSHJTB with different relief hole distributions. Type A refers to EPSHJTB with radial relief holes only, while type B refers to EPSHJTB with thrust relief holes only.

Figure 13 demonstrates the pressure distribution contour of model A with type A and type B. Figure 14 presents the pressure distribution curve in the thrust gas film. It is found that the type B owns the lower thrust gas film outlet back pressure, which achieves the higher pressure difference between main thrust bearing surface and auxiliary thrust face. Therefore, the axial load capacity of type B is larger, which is 8244.17 N, as shown in Table 6. Figure 15 compares the temperature distribution of main thrust face type A and type B.

Figure 16 displays the pressure distribution contour of model B with type A and type B. Figure 17 shows the pressure distribution curve in the axial middle position of the radial gas film. It is found that the maximum average gas film pressure of type A is about 2.825 MPa and the minimum pressure is about 2.59 MPa. Besides, maximum average gas film pressure of type B is about 2.915 MPa and the minimum average gas

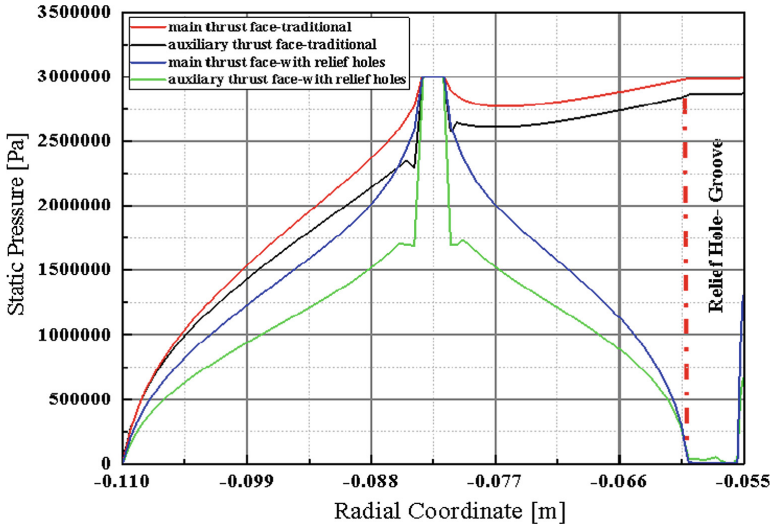


Fig. 11. Curve of thrust film pressure distribution-EP SHJT B with relief holes

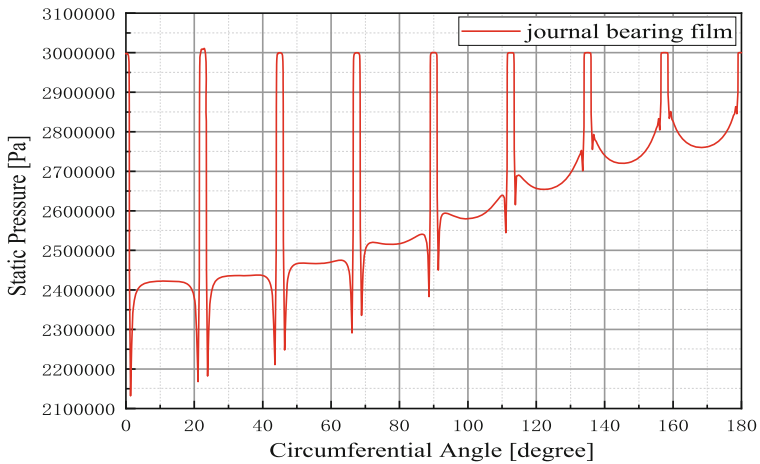


Fig. 12. Circumferential distribution of journal bearing film pressure-EP SHJT B with relief holes

Table 5. Comparison of load capacity and mass flow

Bearing Type	Axial Force/N	Radial Force/N	Mass Flow/(kg/s)
Traditional	3332.40	0.00	0.0056512
Relief Holes	8259.00	2875.90	0.043208

film pressure is about 2.8 MPa. The pressure difference of type A is larger. Therefore, the radial load capacity of type A is larger, which is 1843.89 N, as shown in Table 6. Figure 18 illustrates the temperature distribution curve in the axial middle position of the radial gas film. And This temperature distribution is also similar to pressure distribution. Taken together, EPSHJTB with radial relief holes only-type A has the smaller axial force and the larger radial force compared with type B.

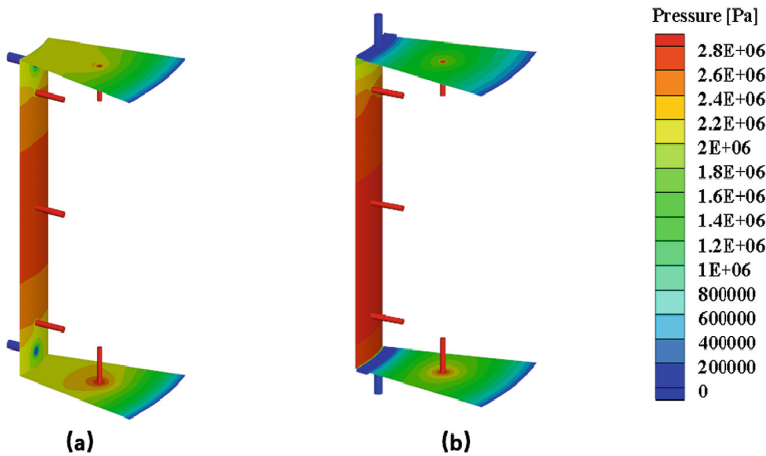


Fig. 13. Pressure distribution contour of EPSHJTB with relief holes: **a** Type A-with radial relief holes only; and **b** Type B-with thrust relief holes only

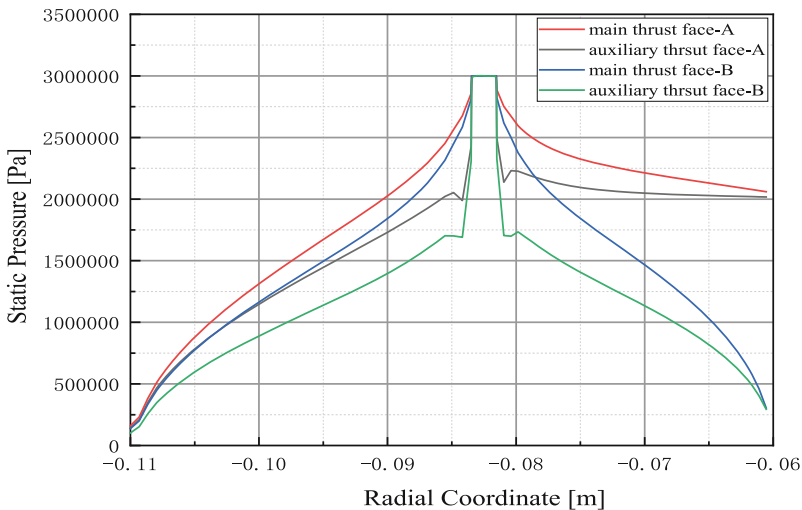


Fig. 14. Curve of thrust film pressure distribution

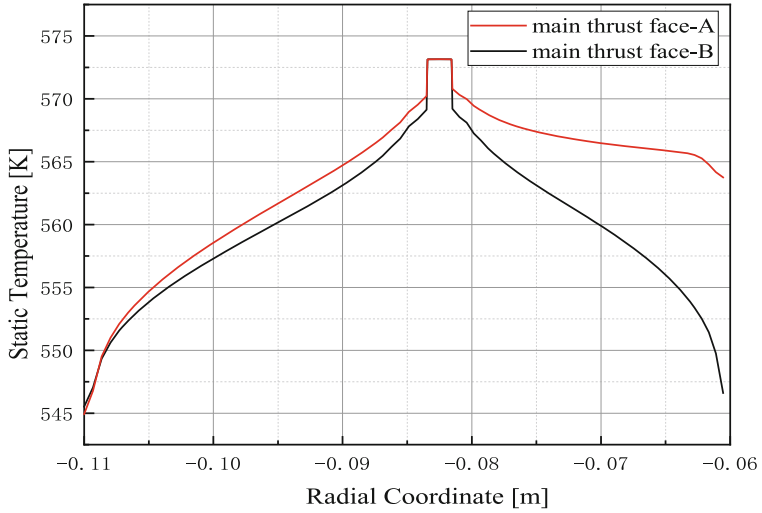


Fig. 15. Curve of thrust film temperature distribution

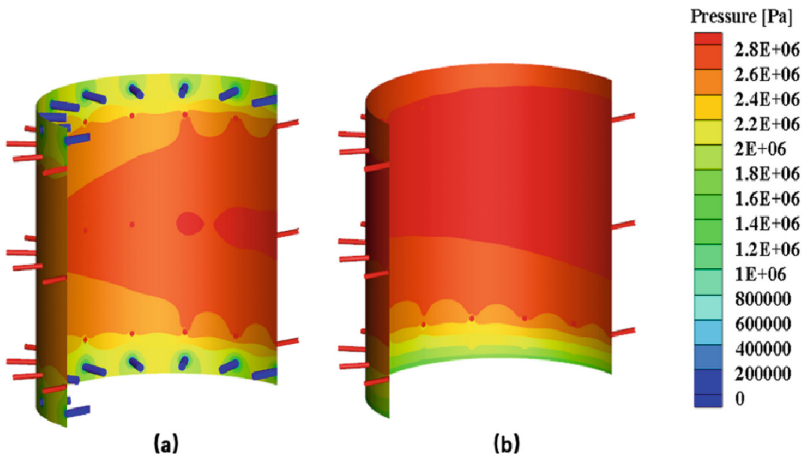


Fig. 16. Pressure distribution contour of EPSHJTb with relief holes: **a** Type A-with radial relief holes only; and **b** Type B-with thrust relief holes only

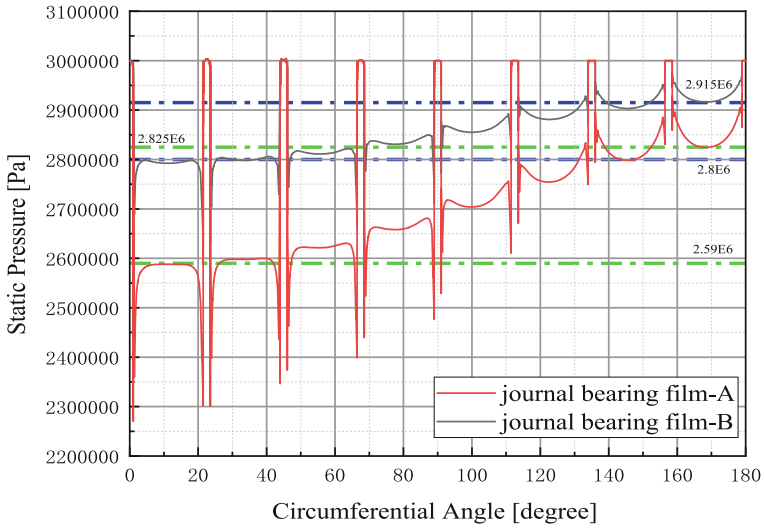


Fig. 17. Circumferential distribution of journal bearing film pressure

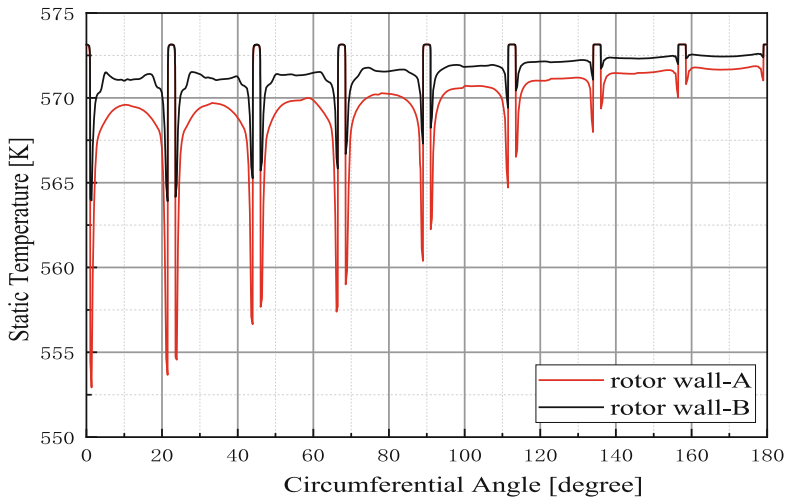


Fig. 18. Circumferential distribution of journal bearing film temperature

Table 6. Comparison of load capacity and mass flow

Bearing Type	Axial Force/N	Radial Force/N		Mass Flow/(kg/s)
All relief holes	8259.00	2875.90		0.043208
Type-A	4685.41	1843.89		0.037284
Type-B	8244.17		1162.84	0.029134

4 Conclusion

This study sets out to study the flow and load capacity characteristics of externally pressurized steam hybrid journal-thrust bearing (EPSHJTB). It provides advice for improving the load capacity of EPSHJTB.

1. Traditional EPSHJTB has nearly zero radial load capacity due to the high radial gas film outlet back pressure. And the limited axial load capacity is caused by the pressure equalization of high axial gas film outlet back pressure.

2. EPSHJTB with relief holes can improve the load capacity of the traditional EPSHJTB by reducing the radial and axial gas film outlet back pressure.

3. The distribution of relief holes will influence the static performance of EPSHJTB owing to the change of outlet back pressure.

References

1. Olumide, O., Meihong, W., Greg, K.: Closed-cycle gas turbine for power generation: A state-of-the-art review. *Fuel*, 694–717 (2016)
2. Orcutt, F.K., Dougherty, D.E., Malanoski, S.B., et al.: Investigation of externally pressurized steam-lubricated journal bearing. *J Lubr Technol* **90**(4), 723–730 (1968)
3. Rowe, W.B.: *Hydrostatic, aerostatic and hybrid bearing design*. Elsevier, New York (2012)
4. Yates, H.G.: Combined journal and thrust bearings. UK Patent 639, 293, June, 1963 (1950)
5. Lund, J.W.: Static stiffness and dynamic angular stiffness of the combined hydrostatic journal-thrust bearing. Mechanical Technology Inc. Report Number MTI 63 TR45 (1963)
6. Colombo, F., Lentini, L., Raparelli, T., et al.: The challenges of oil free bearings in micro-turbomachinery. In: *Proceedings of I4SDG Workshop 2021: IFToMM for Sustainable Development Goals 1*. Springer International Publishing, pp. 403–411 (2022)
7. Belforte, G., Raparelli, T., Trivella, A., et al.: Discharge coefficients of orifice-type restrictor for aerostatic bearings. *Tribol Int* **40**, 512–521 (2007)
8. Chen, S., Zhang, Q., Fu, B., et al.: Analysis of static and dynamic characteristics of aerostatic bearing with reflux orifices. *Ind Lubr Tribol* **73**(6), 961–970 (2021)
9. Liu, L., Lu, L., Yu, K., et al.: A steady modeling method to study the effect of fluid–structure interaction on the thrust stiffness of an aerostatic spindle. *Eng. Appli. Computat. Fluid Mechan.* **16**(1), 453–468 (2022)
10. Lu, L., Gao, Q., Chen, W., et al.: Investigation on the fluid–structure interaction effect of an aerostatic spindle and the influence of structural dimensions on its performance. In: *Proceedings of the institution of mechanical engineers, part J: journal of engineering tribology* **231**(11), 1434–1440 (2017)
11. Zhang, Z.: Research on static and dynamic characteristics of aerostatic spindal in ultra-precision grinding machine. PhD Thesis. Harbin Institute of Technology, China (2019)

12. Kobayashi, T., Yabe, H.: Numerical analysis of a coupled porous journal and thrust bearing system. *ASME J Tribol* **127**(1), 120–129 (2005)
13. Ise, T., Osaki, M., Matsubara, M., et al.: Vibration reduction of large unbalanced rotor supported by externally pressurized gas journal bearings with asymmetrically arranged gas supply holes (Verification of the effectiveness of a supply gas pressure control system). *ASME J Tribol* **141**(3), 031701 (2019)
14. Du, J., Zhang, G., Liu, T., et al.: Improvement on load performance of externally pressurized gas journal bearings by opening pressure-equalizing grooves. *Tribol Int* **73**, 156–166 (2014)
15. Li, W., Zhang, Y., Cai, S., et al.: Numerical and experimental investigation on the performance of backflow channel aerostatic bearings with shunt injection. *Tribol Trans* **2022**, 1–22 (2022)
16. Li, W., Wang, G., Feng, K., et al.: CFD-based investigation and experimental study on the performances of novel back-flow channel aerostatic bearings. *Tribol Int* **165**, 107319 (2022)
17. Mori, H.: A theoretical investigation of pressure depression in externally pressurized gas-lubricated circular thrust bearings. *J Basic Eng* **83**, 201–208 (1961)
18. Mori, H., Miyamatsu, Y.: Theoretical flow-models for externally pressurized gas bearings. *J Lubr Technol* **91**, 181–193 (1969)
19. Chunyang, N., Yulong, L., et al.: Research on bearing and lubrication technology of heat pump compressor under microgravity. *Manned Spacecraft* **25**(01), 50–55 (2019)
20. Bell, I.H., Wronski, J., Quoilin, S., et al.: Pure and pseudo-pure fluid thermophysical property evaluation and the open-source thermophysical property library CoolProp. *Ind. Eng. Chem. Res.* **53**(6), 2498–2508 (2014)